International Journal of Thermal Sciences 48 (2009) 1967–1977

Contents lists available at ScienceDirect

International Journal of Thermal Sciences

journal homepage: www.elsevier.com/locate/ijts

Multi-objective optimization of rotary regenerator using genetic algorithm

Sepehr Sanaye*, Hassan Hajabdollahi

Energy Systems Improvement Laboratory (ESIL), Department of Mechanical Engineering, Iran University of Science and Technology (IUST), Narmak, Tehran 16844, Iran

ARTICLE INFO

Article history:
Received 18 June 2008
Received in revised form
31 January 2009
Accepted 11 February 2009
Available online 21 March 2009

Keywords:
Rotary regenerator
Effectiveness
Pressure drop
Multi-objective optimization

ABSTRACT

The rotary regenerator (heat wheel) is an important heat recovery equipment, which rotates between two cold and hot streams. The pressure drop and effectiveness of rotary regenerator are important parameters in optimal design of this equipment for industrial applications. For optimal design of such a system, it was thermally modeled using ε-NTU method to estimate its pressure drop and effectiveness. Frontal area, ratio of hot to cold frontal heat transfer area, matrix thickness, matrix rotational speed, matrix rod diameter and porosity were considered as design parameters. Then fast and elitist non-dominated sorting genetic algorithm (NSGA-II) method was applied to find the optimum values of design parameters. In the presented optimal design approach, the effectiveness and the total pressure drop are two objective functions. The results of optimal designs were a set of multiple optimum solutions, called 'Pareto optimal solutions'. The sensitivity analysis of change in optimum effectiveness and pressure drop with change in design parameters of the regenerator was also performed and the results are reported.

1. Introduction

A rotary regenerator as shown in Fig. 1, is a compact heat exchanger with a cylindrical matrix which provides a large heat transfer surface area [1]. Flow passages are generally of cellular structure referred to as a matrix. When the hot gas flows over the heat transfer surface area in flow passages, the hot gas thermal energy stores in the matrix walls. Then during the cold gas flow through the same passages, the matrix wall releases the thermal energy to the cold fluid. Thus, heat is not transferred continuously through the wall as exists in a recuperator, but the thermal energy is alternately stored and released by the matrix wall [2,3]. In order to have continuous operation, the matrix rotates with a part of the matrix in the hot stream and the rest in the cold stream. Ghodsipour [4] estimated the maximum regenerator effectiveness as a function of rotational speed as well as hot and cold air velocities. Wu et al. [5], developed a mathematical model to simulate ventilation air flow control system of an air-conditioning unit including a rotary regenerator. Sanaye et al. [6] obtained optimum operational conditions of air-to-air rotary regenerator for air-conditioning applications considering thermal effectiveness as a single objective function. Hilbert [7] applied a multi-objective optimization technique to maximize the heat transfer rate and to minimize the pressure drop in a tube bank heat exchanger. Foli et al. [8] estimated the optimum geometric parameters of micro channels in micro heat exchangers by maximizing the heat transfer rate and minimizing the pressure drop as two objective functions. Liu and Cheng [9], optimized a recuperator for the maximum heat transfer effectiveness as well as minimum exchanger weight and pressure loss. Gholap [10] also studied air cooled heat exchangers by minimizing the energy consumption of fans and material cost as two objective functions.

In this paper after thermal modeling of an industrial rotary regenerator, this equipment was optimized by maximizing the effectiveness as well as minimizing the pressure drop. Genetic algorithm optimization technique was applied to provide a set of Pareto multiple optimum solutions. The sensitivity analysis of change in optimum values of effectiveness and pressure drop with change in design parameters was performed and the results are reported.

As a summary, the followings are the contribution of this paper in the subject:

- Thermal modeling of rotary regenerators with randomly stacked woven-screen matrix by proposing a closed form equation for predicting the heat transfer coefficient and pressure drop.
- Multi-objective optimization for rotary regenerator with effectiveness and pressure drop as two objectives using genetic algorithm.
- Selecting the frontal area, split, matrix thickness and rotational speed, as well as matrix rod diameter and porosity as design parameters (decision variables).

* Corresponding author. Tel./fax: +98 21 77240192.
E-mail address: sepehr@iust.ac.ir (S. Sanaye).

1290-0729/$ – see front matter © 2009 Elsevier Masson SAS. All rights reserved.
doi:10.1016/j.ijthermalsci.2009.02.008

Nomenclature

A	heat transfer area (m^2)
A_{fr}	flow frontal area (m^2)
A_{cross}	free flow cross-section area (m^2)
c	specific heat (j/kg K)
C	flow stream heat capacity rate (W/K)
C_{min}	minimum of Ch and Cc (W/K)
C_{max}	maximum of Ch and Cc (W/K)
C^*	heat capacity rate ratio (C_{min}/C_{max})
Cr	total heat capacity rate of a matrix (W/K)
Cr^*	matrix heat capacity rate ratio (C_r/C_{min})
d	matrix rod diameter (m)
f	friction factor (–)
G	mass flux (kg/m^2 s)
h	heat transfer coefficient (W/m^2 K)
j	Culburn number (–)
k_w	wall heat conduction coefficient (W/m K)
m	mass flow rate (kg/s)
m_m	matrix mass (kg)
NTU	number of transfer units (–)
N_r	matrix rotational speed (rpm)
Nu	nusselt number
Pr	Prandtl number
Re	Reynolds number
r_h	matrix radius (m)
split	ratio of hot to cold frontal heat transfer area ($A_{fr,h}/A_{fr,c}$)
T	temperature (K)
t	matrix thickness (m)
V	matrix volume (m^3)
x_t	transverse pitch of the rod

Greek abbreviation

Δp	pressure drop (kpa)
α	heat transfer area per unit volume (m^2/m^3)
φ_r	correction factor for rotational speed (–)
φ_c	cleanliness factor (–)
μ	viscosity (pa s)
ε	effectiveness
σ	porosity
ρ_m	matrix density (kg/m^3)

Subscripts

c	cold
h	hot
m	matrix
out	outlet
in	inlet
max	maximum
min	minimum
Par	Parameter

- Proposing a new closed form equation for the pressure drop in term of effectiveness at the optimal design point.
- Showing Pareto optimal solution curves for various mass flow rates of cold stream.
- The distribution of optimal design parameters in variable-population coordinates were given and discussed.
- Performing sensitivity analysis of change in objective functions (ε and Δp) when the optimum design parameters vary.

2. Thermal modeling

In this section a rotary regenerator with radial flow (Fig. 1) is modeled. The studied regenerator had a matrix with randomly stacked woven-screen arrangement shown in Fig. 2.

2.1. Geometrical parameters

The ratio of heat transfer surface area to the total volume named (α) is [11, page 44].

$$\alpha = \frac{A}{V} = \frac{\pi}{d\,x_t} \tag{1}$$

where d is the matrix rod diameter and x_t is transverse pitch of the rods.

By defining the porosity factor (void volume/total volume) in form of:

$$\sigma = 1 - \frac{\pi}{4x_t} \tag{2}$$

and combining relations (1) and (2):

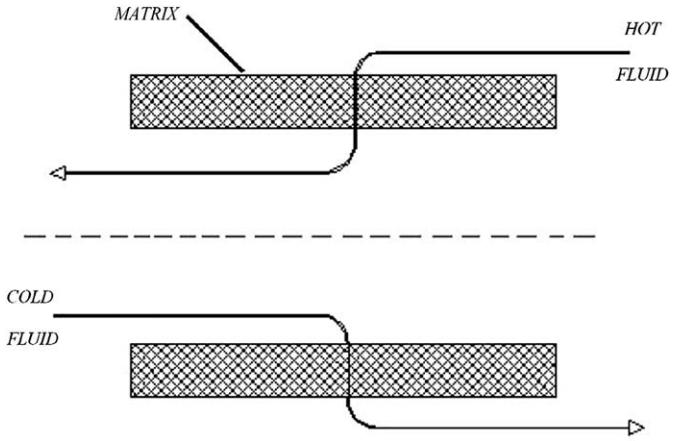

Fig. 1. Rotary regenerator with radial flow.

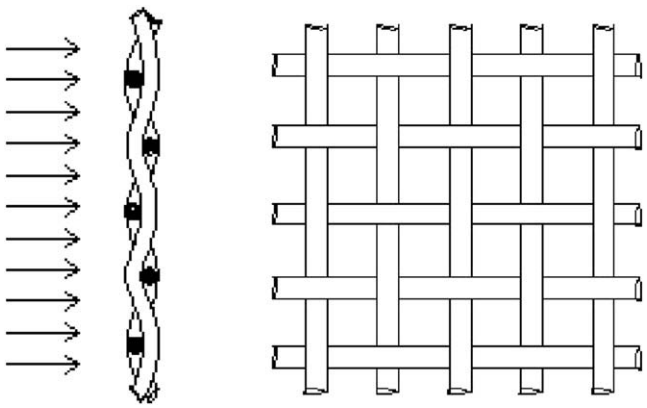

Fig. 2. Randomly stacked woven-screen matrix.

$$\alpha = \frac{4}{d}(1-\sigma) \tag{3}$$

Furthermore the hydraulic radius and split are defined as:

$$r_h = \frac{\sigma}{\alpha} \tag{4}$$

$$\text{split} = \frac{A_{\text{fr,h}}}{A_{\text{fr,c}}} = \frac{A_{\text{h}}}{A_{\text{c}}} \tag{5}$$

where:

$$A_{\text{c}} + A_{\text{h}} = \alpha V \tag{6}$$

and V (the matrix volume) is related to the frontal area (A_{fr}) and matrix thickness (t) as follows:

$$V = A_{\text{fr}} t \tag{7}$$

Therefore A_{c} and A_{h} (heat transfer area) can be obtained from Eqs. (5) and (6).

The free flow cross-section area is also defined as:

$$A_{\text{cross}} = \sigma A_{\text{fr}} \tag{8}$$

2.2. Heat transfer and friction coefficients

The Culburn number and friction factor for randomly stacked woven-screen matrix, shown in Fig. 2, are proposed here as Eqs. (9) and (14) respectively, based on graphical data available in [11, page 148] in form of:

$$j = a(\text{Re})^{-b} + c \tag{9}$$

where a, b and c are constants listed in Table 1 and Reynolds number is computed from:

$$\text{Re} = \frac{4 r_{\text{h}} G}{\mu} \tag{10}$$

where r_{h} is the hydraulic diameter and G is the mass flow rate per flow cross-section area (mass flux):

$$G = \frac{m}{A_{\text{cross}}} \tag{11}$$

Therefore heat transfer coefficient was computed from:

$$h = \text{St} G c \tag{12}$$

where St is Stanton number defined as:

$$\text{St} = \frac{j}{\text{pr}^{2/3}} \tag{13}$$

The friction factor for the mentioned arrangement was also proposed in form of:

$$f = 10^{g(\log(\text{Re}))} \tag{14}$$

$$g(x) = ax^3 + bx^2 + cx + d \tag{15}$$

where a, b, c and d are constants listed in Table 2.

The above proposed correlations for Culburn number and f factor, are accurate within ±2.5% and +3% respectively.

Furthermore, the pressure drop was also estimated from [1, page 36]:

$$\Delta P = \frac{G^2}{2} v_{\text{in}} \left[\left(K_{\text{c}} + 1 - \sigma^2 \right) + 2\left(\frac{v_{\text{out}}}{v_{\text{in}}} - 1 \right) + \left(f \frac{A}{A_{\text{cross}}} \frac{v_{\text{ave}}}{v_{\text{in}}} \right) - \left(1 - \sigma^2 - K_{\text{e}} \right) \frac{v_{\text{out}}}{v_{\text{in}}} \right] \tag{16}$$

where the K_{c} and K_{e} are coefficients of pressure drop at entrance and exit cross-sections respectively and f is the friction factor obtained from Eq. (14).

2.3. ε-NTU analysis

The regenerator effectiveness (ε) was estimated from Eq. (17), in which, ε_0 denotes the effectiveness of a cross-flow heat exchanger, ϕ_{r}, is a correction factor for rotational speed and ϕ_{c}, represents a correction factor for the cleanliness [12] with the value of one in this study:

$$\varepsilon = \varepsilon_0 \varphi_{\text{r}} \varphi_{\text{c}} = \frac{q}{q_{\max}} = \frac{C_{\text{h}}}{C_{\min}} \frac{(T_{\text{h,in}} - T_{\text{h,out}})}{(T_{\text{h,in}} - T_{\text{c,in}})} = \frac{C_{\text{c}}}{C_{\min}} \frac{(T_{\text{c,out}} - T_{\text{c,in}})}{(T_{\text{h,in}} - T_{\text{c,in}})} \tag{17}$$

The correlation for effectiveness of a cross-flow heat exchanger is [11, page 19]:

$$\varepsilon_0 = \frac{1 - e^{[-\text{Ntu}(1-C^*)]}}{1 - C^* e^{[-\text{Ntu}(1-C^*)]}} \tag{18}$$

where the heat capacity ratio (C^*), and the number of transfer units (NTU), are defined as:

$$C^* = \frac{C_{\min}}{C_{\max}} \tag{19}$$

$$\text{NTU} = \left[\frac{1}{C_{\min}} \right] \left[\frac{1}{1/(h_{\text{c}} A_{\text{c}}) + 1/(h_{\text{h}} A_{\text{h}})} \right] \tag{20}$$

Furthermore the correction factor for the rotational speed (φ_{r}) was obtained in terms of the exchanger heat capacity ratio ($\text{Cr}^* = (\text{Cr}/C_{\min})$) in form of [11, page 32]:

$$\varphi_{\text{r}} = 1 - \frac{1}{9 C_{\text{r}}^{*1.93}} \tag{21}$$

where C_{r} is the total heat capacity rate of the matrix defined as:

$$C_{\text{r}} = (N_{\text{r}}/60) m_{\text{m}} c_{\text{m}} \tag{22}$$

Table 1
The constant coefficients for Eq. (9).

Porosity	a	b	c
0.602	0.5209	0.4072	0.0003504
0.725	0.7568	0.4358	0.001605
0.766	0.9237	0.4479	0.001927
0.832	1.904	0.5413	0.005905

Table 2
The constant coefficients for Eq. (14).

Porosity	a	b	c	d
0.602	−0.03374	0.3851	−1.614	1.988
0.725	−0.0283	0.3477	−1.524	1.739
0.766	−0.03269	0.398	−1.709	1.994
0.832	−0.04621	0.552	−2.258	2.688

N_r is matrix rotational speed and m_m is the matrix mass computed from:

$$m_m = \rho_m(1-\sigma)V \tag{23}$$

2.4. Influence of longitudinal heat conduction

To evaluate the influence of heat conduction in the flow direction either in the solid wall or in the fluid, the following approximation for longitudinal conduction analysis has been also performed. Fluids generally have a low thermal conductivity (liquid metal excepted), but the wall conductivity may be quite high. Consequently, only wall-conduction effects will be considered in the following treatment. The influence of longitudinal conduction is to reduce exchanger effectiveness for a given number of transfer units, and this reduction may be quiet serious in exchangers with short flow lengths design for high effectiveness values ($\varepsilon > 90\%$) [11, page 35]. Assuming the temperature difference δT for the hot fluid, is of the same magnitude for the cold fluid ($C_{min}/C_{max} \approx 1$), and also for the wall then the wall temperature gradient is $\delta T/L$, with L being the flow length (the matrix thickness) and the longitudinal heat transfer by conduction is of the order [11, page 34]. If the wall cross-section area for longitudinal conduction is designated A_k:

$$q_{cond} \approx k_w A_k \frac{\delta T}{L} \tag{24}$$

where A_k, is the wall cross-section area for longitudinal conduction and k_w, is the wall conduction coefficient.

The convection heat transfer rate is also given by energy-balance considerations as:

$$q_{conv} = C_c \delta T = C_h \delta T \tag{25}$$

and then

$$\frac{q_{cond}}{q_{conv}} = \frac{(k_w/L)A_k}{C} = \frac{\left(k_w/L\right)A_{fr}(1-\sigma)}{C_{min}} = \lambda \tag{26}$$

where λ in equation (26), is the non-dimensional conduction parameter. The values of λ are computed for various optimal design points as presented in Section 5.1 and Fig. 4.

3. Genetic algorithms for multi-objective optimization

3.1. Objective functions and decision variables

In this study the effectiveness and pressure drop are two objective functions. The goals are to maximize effectiveness while minimizing the pressure drop. Six design parameters or decision variables ($N_{par} = 6$) for the optimization process are frontal area, ratio of hot to cold frontal (split), matrix thickness, matrix rotational speed, matrix rod diameter and porosity.

3.2. Multi-objective optimization

A multi-objective problem consists of optimizing (i.e. minimizing or maximizing) several objectives simultaneously, with a number of inequality or equality constraints. The problem can be formally written as follows:

$$\text{Find } x = (x_i) \quad \forall i = 1,2,\ldots,N_{par} \text{ such as} \tag{27}$$

$f_i(x)$ is a minimum (respectively maximum) $\forall i = 1,2,\ldots,N_{obj}$

Subject to:

$$g_j(x) = 0 \quad \forall j = 1,2,\ldots,M, \tag{28}$$

$$h_k(x) \le 0 \quad \forall k = 1,2,\ldots,K, \tag{29}$$

where x is a vector containing the N_{par} design parameters, $(f_i)_{i=1,\ldots,N_{obj}}$ the objective functions and N_{obj} the number of objectives. The objective function $(f_i)_{i=1,\ldots,N_{obj}}$ returns a vector containing the set of N_{obj} values associated with the elementary objectives to be optimized simultaneously. The GAs are semi-stochastic methods, based on an analogy with Darwin's laws of natural selection [13]. The first multi-objective GA, called vector evaluated GA (or VEGA), was proposed by Schaffer [14]. An algorithm based on non-dominated sorting was proposed by Srinivas and Deb [15] and called non-dominated sorting genetic algorithm (NSGA). This was later modified by Deb et al. [16] which eliminated higher computational complexity, lack of elitism and the need for specifying the sharing parameter. This algorithm is called NSGA-II which is coupled with the objective functions developed in this study for optimization.

3.3. Non-dominated sorting

Following the definition by Deb [17], an individual $X^{(a)}$ is said to constrain-dominate an individual $X^{(b)}$, if any of the following conditions are true:

(1) $X^{(a)}$ and $X^{(b)}$ are feasible, with
   (a) $X^{(a)}$ is no worse than $X^{(b)}$ in all objective, and
   (b) $X^{(a)}$ is strictly better than $X^{(b)}$ in at least one objective.
(2) $X^{(a)}$ is feasible while individual $X^{(b)}$ is not.
(3) $X^{(a)}$ and $X^{(b)}$ are both infeasible, but $X^{(a)}$ has a smaller constraint violation.

(30)

Here, the constraint violation $\ell(X)$ of an individual X is defined to be equal to the sum of the violated constraint function values [18],

$$\ell(X) = \sum_{j=1}^{B} \gamma\left(g_j(X)\right) g_j(X), \tag{31}$$

where γ is the Heaviside step function. A set of non-dominated individuals, to form a Pareto optimal fronts.

3.4. Tournament selection

Each individual competes in exactly two tournaments with randomly selected individuals, a procedure which imitates survival of the fittest in nature.

3.5. Controlled elitism sort

To preserve diversity, the influence of elitism is controlled by choosing the number of individuals from each subpopulation, according to the geometric distribution [19],

$$S_q = S\frac{1-c}{1-c^w}c^{q-1}, \tag{32}$$

to form a parent search population, P_{t+1}(t denote the generation), of size S, where $0 < c < 1$. And w is the total number of ranked non-dominated.

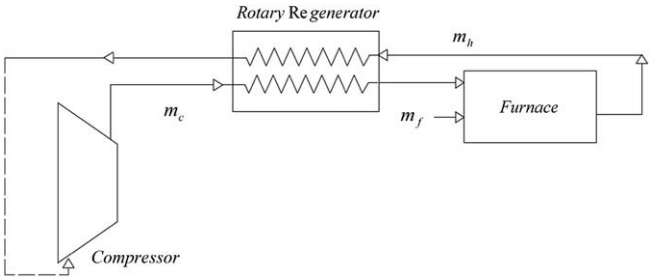

Fig. 3. The schematic diagram of a furnace with a rotary regenerator as preheater.

3.6. Crowding distance

The crowding distance metric proposed by Deb [17] is utilized, where the crowding distance of an individual is the perimeter of the rectangle with its nearest neighbors at diagonally opposite corners. So, if individual $X^{(a)}$ and individual $X^{(b)}$ have same rank, each one has a larger crowding distance is better.

3.7. Crossover and mutation

Uniform crossover and random uniform mutation are employed to obtain the offspring population, Q_{t+1}. The integer-based uniform crossover operator takes two distinct parent individuals and interchanges each corresponding binary bits with a probability, $0 < p_c \leq 1$. Following crossover, the mutation operator changes each of the binary bits with a mutation probability, $0 < p_m < 0.5$.

3.8. Historical archive

The NSGA-II algorithm has been modified to include an archive of the historically non-dominated individuals, H_t. Archive is used to update the data at each iteration.

4. Case study

The regenerator optimum design parameters were obtained for a gas furnace in Sarcheshmeh cupper production plant located in south of Kerman city. The furnace melting load was about 100 ton/h. The furnace includes a compressor with the pressure ratio $r_p = 2$ and regenerator as is shown in Fig. 3. The fresh air passes through the compressor with 12 kg/s mass flow rate and exits from compressor at 400 K. This air then enters the burners after preheating in regenerator. The fuel to air mass ratio in combustion was about 0.08. The regenerator metal was from stainless steel with thermal conductivity and density listed in Table 3. Thermophysical properties of air such as Prandtl number, viscosity and specific heat were considered to be as temperature dependent.

Table 3
Input values for comparison of modeling results with results from reference [1, page 320].

Split	2.5
Frontal area	3.47 (m^2)
Matrix thickness	0.021 (m)
Matrix rotational speed	26.5 (rpm)
Matrix rod diameter	0.34 (mm)
Porosity	0.725
Mass flow rate of cold flow	9.5 (kg/s)
Fuel to air mass ratio	0.015 (kg/kg)
Inlet hot temperature	948 (K)
Inlet cold temperature	441 (K)
Inlet pressure (cold side)	0.329 (MPa)
Inlet pressure (hot side)	0.105 (MPa)
Matrix metal density	7817 (kg/m^3)
Matrix metal specific heat	500 (J/kg K)

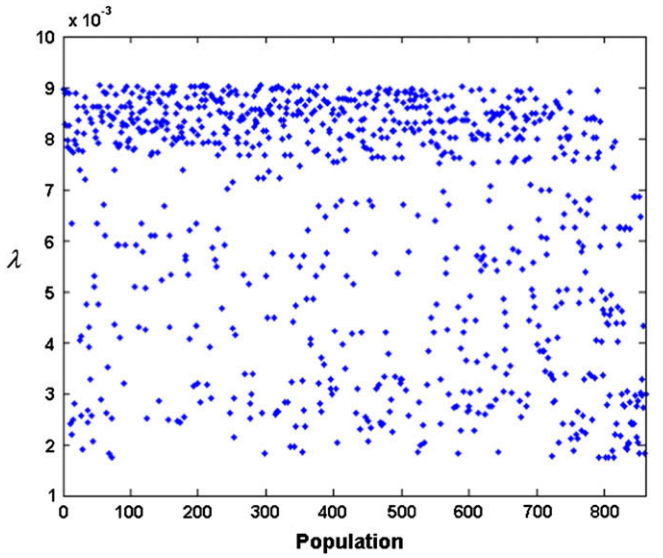

Fig. 4. The distribution of numerical values of λ (the non-dimensional heat conduction parameter) in the whole optimal output domain.

5. Discussion and results

5.1. Longitudinal heat conduction

To quantify the effect of longitudinal heat conduction in comparison with the convection heat transfer, the numerical values of λ (equation (26)) were computed for $k_w = 16.5$ W/m k for all optimum design cases as is shown in Fig. 4. It was found that the distribution of λ value in the whole optimal output domain show the numerical values less than 0.009 (0.9%). This shows that assuming the negligible conduction heat transfer in our analysis in flow direction is acceptable for the studied problem.

5.2. Verification of modeling results

To verify the modeling results, the simulation output was compared with the corresponding reported results given in the literature. The comparison of our modeling results and the corresponding values from reference [11, page 320], is shown in Table 5. Results show that for the same input values listed in Table 4, the difference percentages of output results, are acceptable.

Table 4
Comparison of modeling outputs and the corresponding results from reference [1, page 320].

Output variables	Unit	Ref. [1, page 320]	Present paper	Difference (%)
j_h		0.088	0.0913	3.75
f_h		0.64	0.6296	−1.625
j_c		0.057	0.0592	3.86
f_c		0.46	0.4342	−5.6
h_h	(W/m^2 K)	687	679	−1.16
h_c	(W/m^2 K)	1050	1071.2	2.02
ε		82	81.61	−0.476
Δp_h	(kPa)	1.753	1.714	−2.21
Δp_c	(kPa)	2.273	2.066	−9.1

Table 5
The design parameters and their range of variations for input values given in Table 3.

Variables	From	To	Step of change
Split	1/3	3	0.01
Frontal area (m^2)	3	4	0.01
Matrix thickness (m)	0.1	0.5	0.001
Matrix rotational speed (rpm)	1	10	0.01
Matrix rod diameter (mm)	3	10	–
Porosity	0.602	0.832	–

5.3. Optimization results

To maximize the effectiveness value and to minimize the pressure drop (two objective function), six design parameters including frontal area, ratio of hot to cold frontal (split), matrix thickness, matrix rotational speed, matrix rod diameter and porosity were considered. Design parameters (decision variables) and the range of their variations are listed in Table 6. Four porosity values (0.602,0.725,0.766,0.832) and ten matrix rod diameter (3,3.5,4,4.5,5,6,7,8,9,10 mm) were among the options.

The genetic algorithm optimization was performed for 100 generations, using a search population size of $M = 100$ individuals, crossover probability of $p_c = 0.9$, gene mutation probability of $p_m = 0.035$ and controlled elitism value $c = 0.55$.

The number of iterations for finding the global extremum in the whole searching domain was about 3.85×10^{11}.

The results for Pareto optimal curve are shown in Fig. 5, which clearly reveals the conflict between two objectives, the effectiveness and the pressure drop. Any geometrical change that increases the effectiveness or heat transfer rate ($\varepsilon = q/q_{max}$), leads to an increase in the pressure drop and vice versa, which shows the need for multi-objective optimization techniques in optimal design of a rotary regenerator. It is shown in Fig. 5, that the maximum effectiveness exists at design point A (0.9229), while the pressure drop is the biggest at this point. On the other hand the minimum pressure drop occurs at design point F, with an unacceptable effectiveness value (0.08678) at that point. Design point A is the optimal situation at which, efficiency is a single objective function, while design point F is the optimum condition at which pressure drop is a single objective function. Specifications of six sample design points A–F in Pareto optimal fronts are listed in Table 6.

As the optimized points in the A–B region have the maximum effectiveness increment 7.1% and minimum pressure drop increment 139.86% relative to the design C, this region was eliminated from the Pareto curve remaining just the region of C–F as shown in Fig. 6.

Distribution of variables of Pareto curve (Fig. 5) is shown in Fig. 7a–f. Lower and upper bounds of the variables shown by dotted lines.

The following points for the optimal variables in Fig. 7 could be deduced:

1. The numerical values of the frontal area are usually at their maximum level.
2. The split values are distributed in the margin of $1.03 < \text{split} < 1.66$.

Table 6
Optimum design values for A to E Pareto optimal fronts for input values given in Table 3.

	A	B	C	D	E	F
Effectiveness	0.9229	0.8636	0.8617	0.7572	0.6	0.08687
Matrix volume (m^3)	1.9929	1.2078	1.9633	1.9711	0.943	0.4
Total pressure drop (kPa)	30.17	18.28	7.621	3.638	1.721	0.1928
Rate of heat transfer (MW)	7.7978	7.2636	7.2469	6.3151	4.7659	0.6919

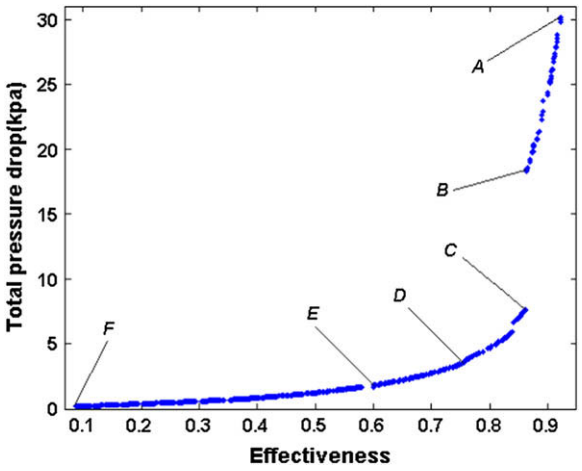

Fig. 5. The distribution of Pareto optimal points solutions.

3. The matrix thickness has the values distributed equally in its whole allowable domain.
4. The rotational matrix velocity is always at its maximum values.
5. The matrix rod diameter has its values distributed in whole allowable region.
6. The porosity has scattering distribution.

Since the matrix thickness, matrix rod diameter and porosity have scattered distribution in their whole allowable domains, one may predict that these three parameters have important effects on the conflict between higher values of effectiveness and lower amounts of pressure drop. Furthermore due to relative scattered characteristic of split, it was expected that the value of split causes a relatively weaker conflict between the maximum and minimum values of two objective functions.

5.4. Effectiveness and pressure drop

To provide a very helpful tool for the optimal design of the regenerators, the following equation was derived for the Pareto optimal points curve (Fig. 6).

$$\Delta p = \frac{-6890\varepsilon^2 + 5666\varepsilon + 549.3}{\varepsilon^3 + 6183\varepsilon^2 - 11960\varepsilon + 5753} \tag{33}$$

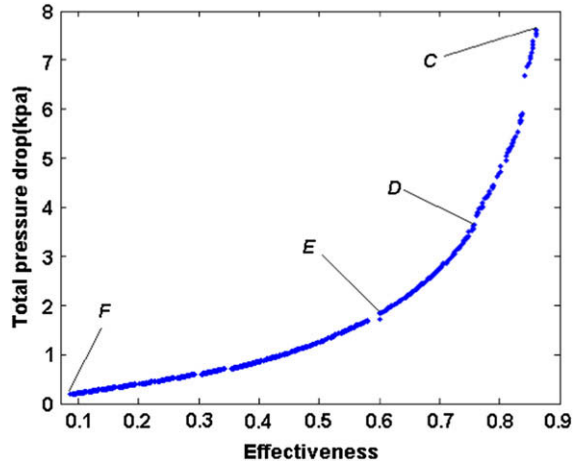

Fig. 6. Pareto optimal points curve for design C–F.

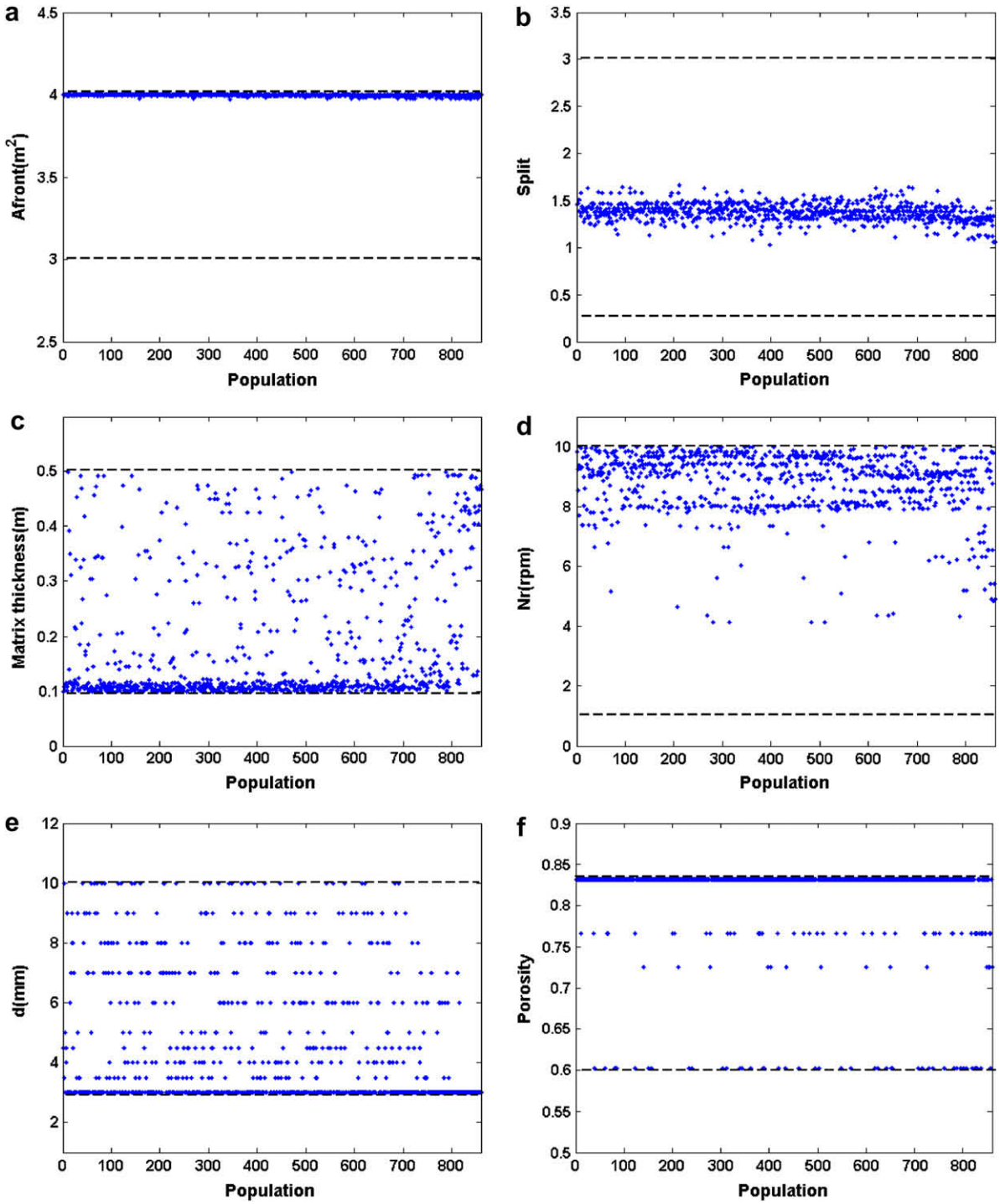

Fig. 7. The distribution of variables for the Pareto curve in the whole optimal design domain.

Equation (33) is valid in the range of $0.086 < \varepsilon < 0.86$ for effectiveness. The interesting point in equation (33) is that considering a numerical value for the effectiveness in the mentioned range, provides the minimum pressure drop for that option along with the values for other optimal design parameters.

Pareto optimal points curve is also shown for various cold air mass flow rates in Fig. 8. As is shown there is a conflict between effectiveness and pressure drop for different mass flow rates, also the curve slope is higher in bigger effectiveness values and mass flow rates. Furthermore for the specific pressure drop, the smaller mass flow rate provided the bigger effectiveness values. The correction factor φ_m for equation (33), for the flow rate in the range of $5 \le m_c \le 12$ is recommended in this paper as:

$$\Delta p^* = \varphi_m \Delta p \tag{34}$$

$$\varphi_m = 1 - 0.237(12 - m_c)^{0.67} \tag{35}$$

To select one of the optimum points from Pareto optimal curve, designs (E–D) are recommended. The design D with higher

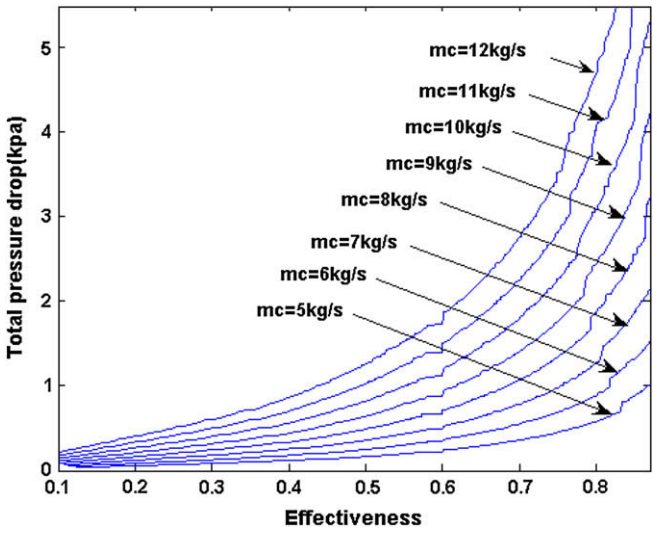

Fig. 8. Pareto optimal points curves for different mass flow rates of cold air.

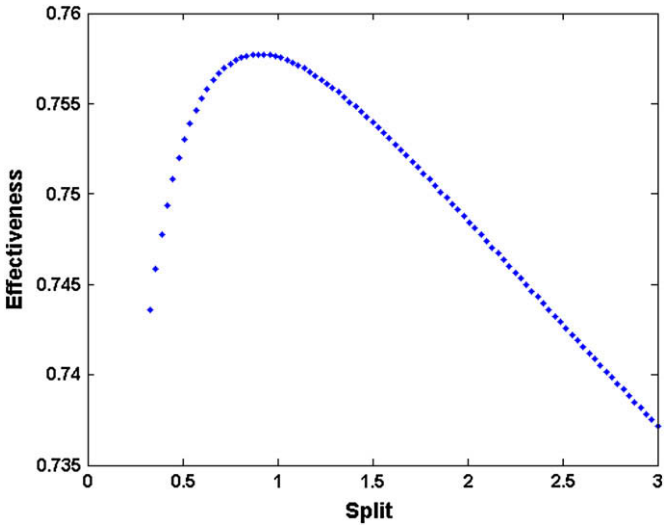

Fig. 10. Variation of effectiveness versus split.

effectiveness value was chosen for our case study, and the effects of variation of design parameters on effectiveness and pressure drop were studied at the design point D.

5.5. The frontal area

Variations of effectiveness versus total pressure drop and frontal area are shown in Fig. 9. Increase in frontal area not only increases the effectiveness but also decreases the pressure drop. The reason can be declared as below:

By increasing A_{fr}, due to the fact that $A_{fr} \propto A$ and $A_{fr} \propto A_{cross}$, the heat transfer surface area A, and the free flow cross-section area A_{cross}, increases. Furthermore the heat transfer coefficient is proportional to $h \propto (aRe^{-b} + c/A_{fr})$ (Eqs. (9) and (12)), therefore from Eq. (10), $(hA)_h$ or $(hA)_c$ is proportional to:

$$hA \propto \left(\frac{aRe^{-b}+c}{A_{fr}}\right)A_{fr} = aRe^{-b} + c \propto aA_{fr}^{+b} + c \tag{36}$$

where a, b and c are positive numbers. Therefore increasing the frontal area increases the number of heat transfer units (Eq. (20)) and effectiveness.

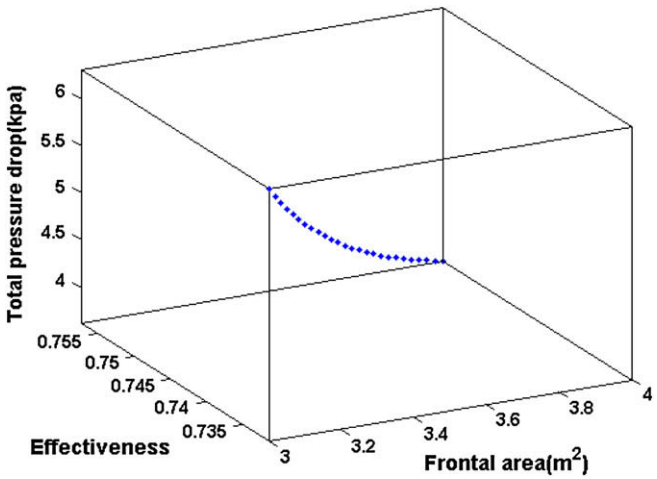

Fig. 9. Variation of effectiveness versus total pressure and frontal area.

On the other hand with increasing A_{fr}, the pressure drop decreases as Eqs. (16) and (36) show:

$$\Delta p \propto G^2 \propto \frac{1}{A_{fr}^2} \tag{37}$$

Due to the above reasons, the maximum frontal area is desired. Scattering distribution of frontal area in Fig. 7a verifies this point too.

5.6. The split

Variations of split versus effectiveness and total pressure drop for design D are shown in Figs. 10 and 11 respectively. By increment of split to its maximum value from 0.33 to 3, equations (36) and (20) show that, the effectiveness increases first (when split < 1 and $A_{fr,h} < A_{fr,c}$) and decreases next (when split > 1 and $A_{fr,h} > A_{fr,c}$) as is shown in Fig. 10. Therefore the maximum effectiveness values occur when:

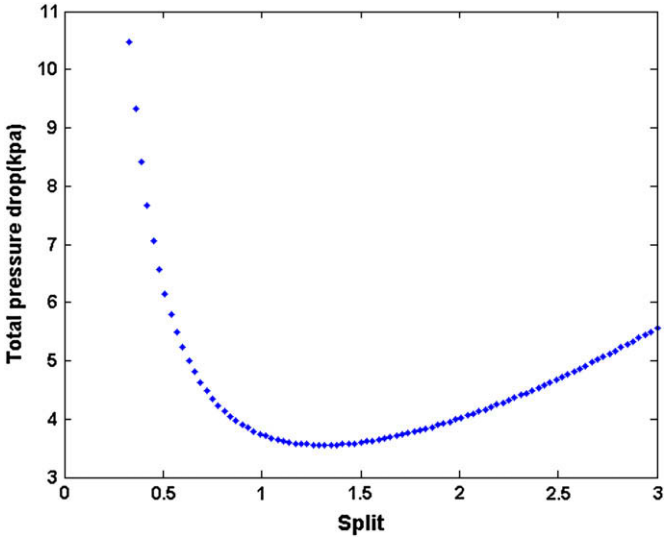

Fig. 11. Variation of total pressure drop versus split.

$$\begin{cases} \forall (m_h > m_c) \Rightarrow \text{split} < 1 \\ \forall (m_h < m_c) \Rightarrow \text{split} > 1 \\ \forall (m_h = m_c) \Rightarrow \text{split} = 1 \end{cases} \quad (38)$$

In our case study in which, $(m_h/m_c) = 1.08 > 1$, the maximum effectiveness occurs in split <1 (Fig. 10). The variations of total pressure drop versus split and effectiveness are shown in Figs. 11 and 12. By increment of split, both effectiveness and total pressure drop increase within a margin (for design point D $0.95 < \text{split} < 1.29$, the hallow circles in Fig. 12). Therefore for design point D, variations of split causes a conflict between two objective functions and the values of split have scattered distribution in the range of $1.03 < \text{split} < 1.66$ (Fig. 7b).

5.7. The matrix thickness

The total pressure drop change versus effectiveness is shown in Fig. 13. By increment of matrix thickness the matrix volume, heat transfer surface area (Eq. (6)), effectiveness (Eq. (20)) and pressure drop (Eq. (16)), increase. Therefore there is a conflict between two objectives function (pressure drop and effectiveness) in this case. This conflict causes scattered distribution at optimum designs point as shown by Fig. 7c.

5.8. The matrix rotational speed

At the optimum design point D, the variation of effectiveness with matrix rotational speed is shown in Fig. 14. At zero rotational speed, there was no heat exchange and thermal effectiveness was zero. Then effectiveness increased sharply up to 1 rpm rotational speed. After 3 rpm, the effectiveness did not change with rpm. Increasing the rotational speed resulted in increasing the non-dimensional parameter Cr^*, which increases the thermal effectiveness. On the other hand by increasing the rotational speed the air mass flow rate passing through matrix decreases, this phenomenon decreases the thermal effectiveness. Two above mentioned counter effects, resulted the flat curves of effectiveness after rotational speed about 3 rpm. The obtained trend of variation of ε with rotational speed was also verified by data provided in references [11, page 33,6]. Results show that there was no significant change in the total pressure drop with variation of rotational speed. Therefore, as shown in Fig. 7d, the rotating speed was just restricted due to keeping the system mechanically in balance.

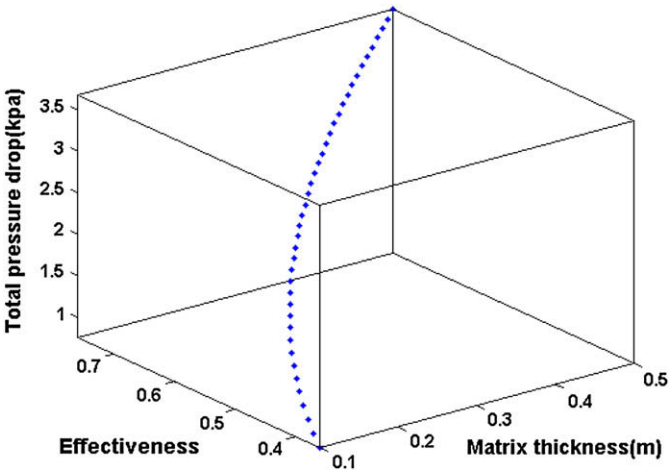

Fig. 13. Variations of effectiveness versus total pressure drop and matrix thickness.

5.9. The matrix rod diameter

By increasing the matrix rod diameter the hydraulic diameter and Reynolds number increase (Eqs. (3) and (4)). An increment in Reynolds number, causes the heat transfer coefficient to decrease (Eqs. (9) and (12)). On the other hand the increment of matrix rod diameter decreases the heat transfer surface area (Eqs. (3) and (6)), then $(hA)_c$ or $(hA)_h$ as well as the number of heat transfer units and finally effectiveness decrease.

By increasing the heat transfer surface area and Reynolds number, the friction coefficient and pressure drop decrease (Eq. (16)). The variations of effectiveness versus pressure drop for the optimum design point D and twelve matrix rod diameters are shown in Fig. 15. By decreasing the matrix rod diameter the effectiveness and the pressure drop both increase. Therefore the matrix rod diameter causes a conflict between the effectiveness and pressure drop, and each rod diameter specifies one point on Pareto optimal points curve.

5.10. Influence of porosity

By increasing the porosity the void spaces and pressure drop decrease. On the other hand decrement of void spaces decreases

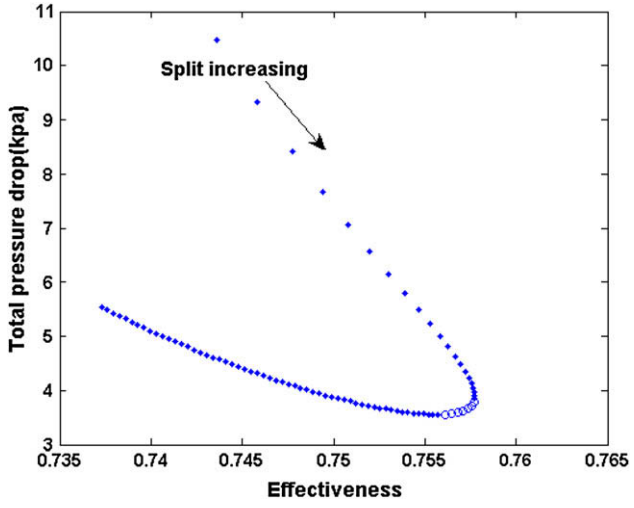

Fig. 12. Variations of effectiveness versus total pressure drop for various amounts of split.

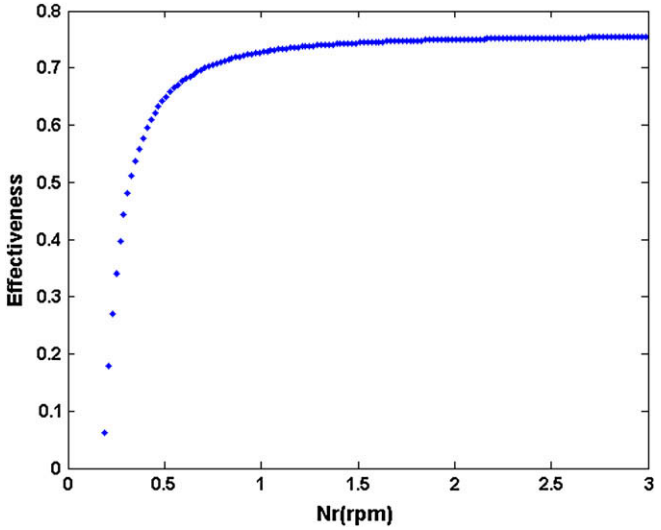

Fig. 14. Variations of effectiveness versus matrix rotational speed.

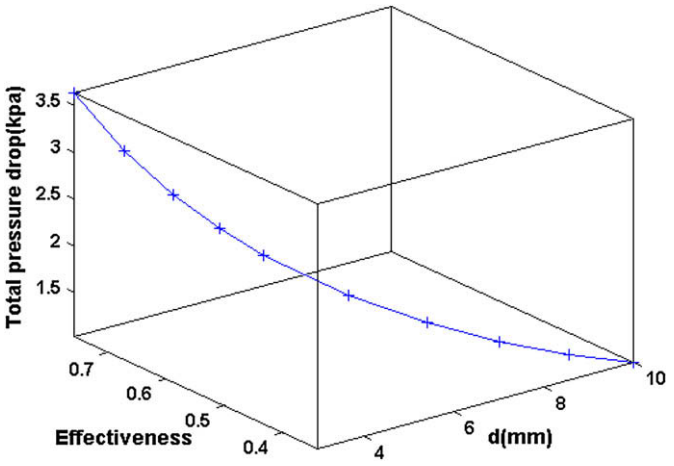

Fig. 15. Variations of effectiveness and pressure drop versus matrix rod diameter.

the compactness factor (ratio of heat transfer surface area to heat exchanger volume) and effectiveness. Therefore porosity also causes a conflict between our two objective functions. As illustrated in Fig. 7f, the bigger porosities the more conflict between objective functions as is shown in Fig. 16.

5.11. Air outlet temperature

The main goal of this paper is to optimally design a rotary regenerator for high temperature applications. The air outlet temperature then may be obtained by computing $T_{c,out}$ from equation (17) (for specific maximized ε). Fig. 17 shows all possible $T_{c,out}$ values at optimal design points. By choosing a specified $T_{c,out}$, all optimal design parameters are then provided.

Therefore when a rotary regenerator with the six optimum decision variables is designed, its ε and N_r, as well as its maximum air outlet temperature are known.

This implies that for each optimal design case (including a specific matrix rotation rate, N_r), there is a unique air outlet temperature for rotary regenerator.

However, one may change and control the air outlet temperature just with change in number of rotation (N_r) (as far as all other design parameters are fixed after manufacturing). At this situation,

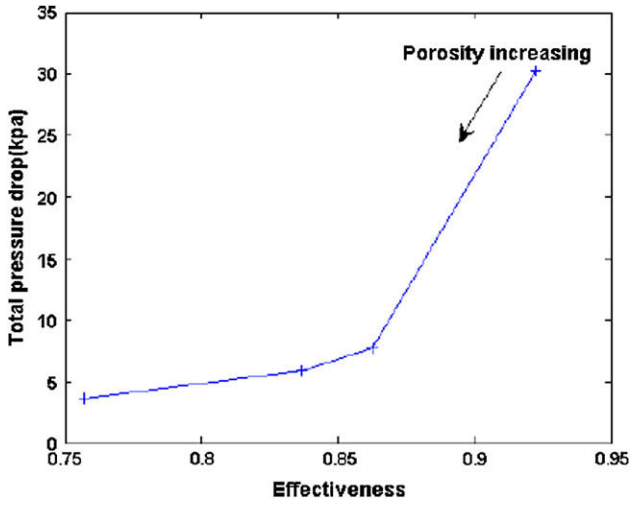

Fig. 16. Variations of effectiveness and pressure drop versus porosity.

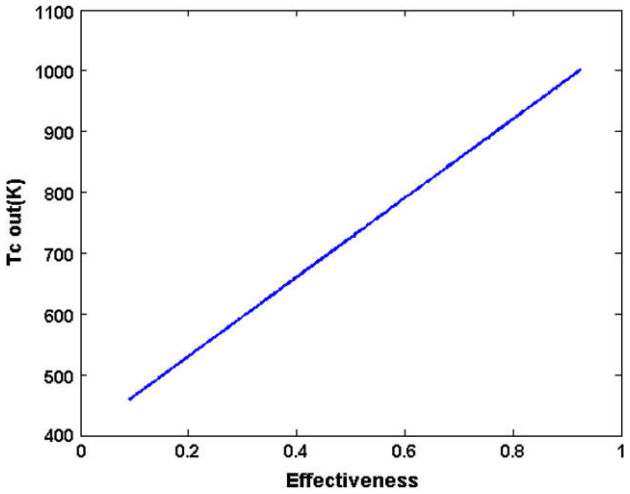

Fig. 17. The corresponding cold air stream outlet temperature for various effectiveness values.

the system is not at optimal design operating condition (a different value of N_r from $N_{r,optimal}$).

In this case by choosing the air outlet temperature, $T_{c,out}$, the ε value can be obtained from equation (17), and the corresponding N_r, can be computed from equation (22) applying equations (17)–(23). It should be noticed that the latter computed ε and N_r values are not optimal values for the manufactured rotary regenerator.

6. Conclusions

A rotary regenerator was optimally designed using multi-objective functions technique.

The designs parameters (decision variables) were frontal area, ratio of hot to cold frontal area (split), matrix thickness, matrix rotational speed, matrix rod diameter and porosity. In the presented optimization problem, the effectiveness and total pressure drop were two considered objective functions. Therefore effectiveness was maximized and total pressure drop was minimized. A set of Pareto optimal points curves for various mass flow rate of cold stream were shown. The results revealed the level of conflict between the two objectives. Matrix thickness, matrix rod diameter and porosity were found important design parameters that cause conflicting between effectiveness and pressure drop. Split also makes a conflict between two objective functions in a short region of validity. Effectiveness increases with rotational speed up to a certain rpm value after which, no considerable change with rpm was observed.

References

[1] T. Skiepko, R.K. Shah, A comparison of rotary regenerator theory and experimental results for an air preheater for a thermal power plant, Experimental Thermal and Fluid Science 28 (2004) 257–264.
[2] R.K. Shah, P. Sekulic, Fundamental of Heat Exchanger Design, John Wiley & Sons, Inc, 2003.
[3] Z. Wu, et al., Model-based analysis and simulation of regenerative heat wheel, Energy and Buildings 38 (2006) 502–514.
[4] N. Ghodsipour, M. Sadrameli, Experimental and sensitivity analysis of a rotary air preheater for the flue gas heat recovery, Applied Thermal Engineering 23 (2003) 571–580.
[5] Z. Wu, R.V.N. Melnik, F. Borup, Model-based analysis and simulation of airflow control systems of ventilation units in building environments, Building and Environment 42 (2007) 203–217.
[6] S. Sanaye, et al., Optimum operational conditions of a rotary regenerator using genetic algorithm, Energy and Buildings 40 (9) (2008) 1637–1642.

[7] R. Hilbert, et al., Multi-objective shape optimization of a heat exchanger using parallel genetic algorithms, International Journal of Heat and Mass Transfer 49 (2006) 2567–2577.
[8] K. Foli, et al., Optimization of micro heat exchanger: CFD, analytical approach and multi-objective evolutionary algorithms, International Journal of Heat and Mass Transfer 49 (2006) 1090–1099.
[9] Z. Liu, H. Cheng, Multi-objective optimization design analysis of primary surface recuperator for microturbines, Applied Thermal Engineering 28 (2008) 601–610.
[10] A.K. Gholap, J.A. Khan, Design and multi-objective optimization of heat exchangers for refrigerators, Applied Energy 84 (2007) 1226–1239.
[11] W.M. Kays, A.L. London, Compact Heat Exchangers, second ed. McGraw Hill Co, 1984.
[12] R.S. Shah, T. Skiepko, Influence of leakage distribution on the thermal performance of a rotary regenerator, Applied Thermal Engineering 19 (1999) 685–705.
[13] D.E. Goldberg, Genetic Algorithms in Search, Optimization and Machine Learning, Addison-Wesley, Reading, MA, 1989.
[14] J.D. Schaffer, Multiple objective optimization with vector evaluated genetic algorithms, in: Proceedings of the International Conference on Genetic Algorithm and Their Applications, 1985.
[15] N. Srinivas, K. Deb, Multiobjective optimization using nondominated sorting in genetic algorithms, Journal of Evolutionary Computation 2 (3) (1994) 221–248.
[16] K. Deb, et al., A fast and elitist multiobjective genetic algorithm: NSGA-II, IEEE Transactions on Evolutionary Computation 6 (2) (2002) 182–197.
[17] K. Deb, Multi-objective Optimization Using Evolutionary Algorithms, John Wiley and Sons Ltd, Chichester, 2001.
[18] K. Deb, An efficient constraint handling method for genetic algorithms, Computer Methods in Applied Mechanics and Engineering 186 (2000) 311–388.
[19] K. Deb, T. Goel, Controlled elitist non-dominated sorting genetic algorithms for better convergence, in: Proceedings of the First International Conference on Evolutionary Multi-criterion Optimization, Zurich, 2001, pp. 385–399.